inorganics

MDPI

Article

FeNi Confined in N-Doped Carbon as a Highly Efficient Bi-Functional Catalyst for Rechargeable Zn–Air Batteries

Lei Duan [1], Zhili Ren [1], Xiaoling Chen [1,*], Ding Zhang [2,*] and Shoudong Xu [1]

[1] College of Chemical Engineering and Technology, Taiyuan University of Technology, Taiyuan 030024, China; duanlei0813@link.tyut.edu.cn (L.D.); renzhili0661@link.tyut.edu.cn (Z.R.); xushoudong@tyut.edu.cn (S.X.)
[2] School of Chemical Engineering and Pharmacy, Wuhan Institute of Technology, Wuhan 430205, China
* Correspondence: chenxiaoling@tyut.edu.cn (X.C.); zhangding@tyut.edu.cn (D.Z.)

Abstract: Rechargeable zinc–air batteries (RZABs) are basically dependent on both affordable and long-lasting bifunctional electrocatalysts. A non-precious metal catalyst, a FeNi nanoalloy catalyst (FeNi@NC) with an extremely low metal consumption (0.06 mmol), has been successfully synthesized. It shows a high half-wave potential of 0.845 V vs. RHE for ORR and a low overpotential of 318 mV for OER at 10 mA cm^{-2}, favoring a maximum power density of 116 mW cm^{-2} for the constructed RZABs. The voltage plateau is reserved even after 167 h of cell operation. The synergistic effect between the nano-sized FeNi alloy and nitrogen-doped carbon with abundant N sites mainly contributes to the electrocatalytic activity. This research can provide some useful guidelines for the development of economic and efficient bifunctional catalysts for RZABs.

Keywords: rechargeable Zn–air batteries; iron–nickel alloy; nitrogen-doped carbon

Citation: Duan, L.; Ren, Z.; Chen, X.; Zhang, D.; Xu, S. FeNi Confined in N-Doped Carbon as a Highly Efficient Bi-Functional Catalyst for Rechargeable Zn–Air Batteries. *Inorganics* **2023**, *11*, 300. https://doi.org/10.3390/inorganics11070300

Academic Editor: Christian Julien

Received: 23 June 2023
Revised: 11 July 2023
Accepted: 12 July 2023
Published: 14 July 2023

1. Introduction

The rising consumption of fossil fuels results in increasing greenhouse gas emissions, highlighting the significance of applying sustainable energy conversion and storage technologies to save energy and protect the environment [1]. Rechargeable zinc–air batteries (RZABs) have stimulated enthusiasm for their high theoretical energy density and low cost. However, such RZABs rely on well-designed catalyzing electrodes that promote oxygen reduction reactions (ORR), oxygen evolution reactions (OER), and diffusion processes. However, the sluggish kinetics of these two processes make it challenging to construct high-performance RZABs. Most current catalysts for RZABs are based on precious metals like platinum and ruthenium, and thus the high cost and restricted reserves prevent them from being widely adopted [2,3]. Therefore, it is necessary to develop dual-functional catalysts with high stability and efficiency.

Transition metal catalysts are viewed as potential candidates for high-performance ORR or OER [4–9]. Iron-based electrocatalysts in particular are among the best options for ORR because of their low cost and superior catalytic activity [10,11], while nickel-based materials have shown excellent catalytic activity for OER [12]. Therefore, a plausible solution for effective bifunctional oxygen electrocatalysts is to make use of the synergy between nickel and iron [7,13–16].

Combining transition metals with doped carbon is a successful method for enhancing bifunctional OER/ORR electrocatalysts, and the most frequently employed doping elements are N, B, F, P, and S. Since N has a higher electronegativity than carbon (C), it is often thought to be the most efficient doping element when used to increase the catalytic activity of ORR and OER compared to other elements [17]. The catalytic activity of ORR/OER is improved when carbon materials are doped with N because the positive charge around the carbon atom lowers the energy barrier for oxygen adsorption, making oxygen chemisorption and electron transfer easier [18–20].

Another simple strategy is to load alloy particles into porous structures. For example, Sun et al. [7] used a simple, template-free method to prepare a novel, non-precious metal-based bifunctional catalyst (Fe_xNi_yN@C/NC) with a porous structure that exposes more active sites and facilitates transport. Zou et al. [5] synthesized alloy catalysts anchored on nitrogen-doped, porous carbon nanosheets by a self-growth strategy (FeCo/NUCSs). Due to the unique structure, the FeCo/NUCS material shows an efficient charge transfer process ($4e^-$), reaction kinetics, and catalytic stability of ORR/OER, resulting in an excellent charge/discharge cycle stability (102 h) in RZABs.

Here, we outline an easy method for creating a N-doped carbon supported FeNi alloy as a bifunctional catalyst. The process includes uniformly binding the metal ions with α-D-glucose, and create M-N_x for catalyzing activity. The optimized catalyst sample shows a high half-wave potential of 0.845 V vs. RHE for ORR and a low overpotential of 318 mV for OER at 10 mA cm^{-2}, favoring a maximum power density of 116 mW cm^{-2} for the constructed RZABs.

2. Experimental

2.1. Synthesis of g-C_3N_4

The urea (8 g) is pyrolyzed in a porcelain boat for 4 h at a heating rate of 5 °C/min. The resulting g-C_3N_4 powder is the final product.

2.2. Synthesis of the Electrocatalysts

The synthesis process of FeNi@NC is illustrated in Figure 1. To prepare FeNi@NC, a mixture of $Ni(NO_3)_2{\cdot}6H_2O$ (0.036 mmol), $Fe(NO_3)_3{\cdot}9H_2O$ (0.024 mmol), 120 mg α-D-glucose, and 1 g g-C_3N_4 was added to deionized water and sonicated for 4 h. The resulting mixture was then stirred for 12 h and dried. The dried mixture was forged for 1 h at 900 °C under an Ar atmosphere using a heating rate of 5 °C/min. The synthesis process for Ni@NC and Fe@NC is identical to that of FeNi@NC.

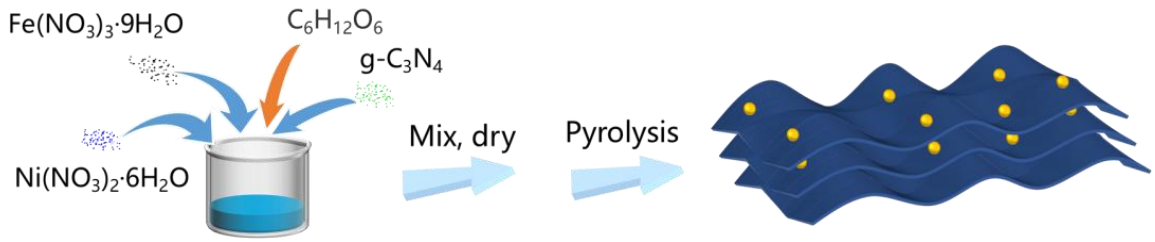

Figure 1. Synthetic steps of FeNi@NC.

The chemicals, characterizations, electrochemical experiments, and Zn–air battery test were summarized in Supporting Information (SI).

3. Results and Discussion

3.1. Preparation and Physicochemical Characterizations

The pyrolysis pathway of FeNi@NC is depicted in Figure 1, where g-C_3N_4 serves as the nitrogen source and α-D-glucose acts as a chelating agent and carbon source [21]. N-doped carbon nanosheets (NC) are created when α-D-glucose undergoes carbonization at 900 °C. At the same time, metal salts comprising Ni^{2+} and Fe^{3+} are changed into FeNi nanoparticles, which are then implanted in the NC carriers. Transmission electron microscopy (TEM) and scanning electron microscopy (SEM) were used to analyze the electrocatalyst's shape and structure. The nanosheets are extremely thin, folded, and have a homogeneous distribution of metal particles on their surface, as shown in Figure 2a, demonstrating a good structural connection.

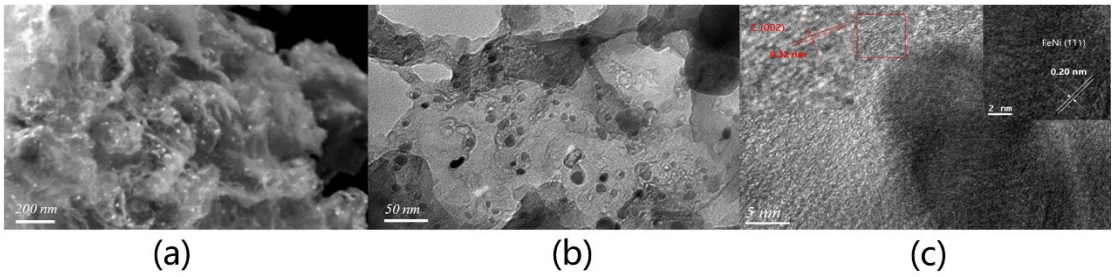

Figure 2. (**a**) SEM and (**b**) TEM images of FeNi@NC. (**c**) HRTEM images of FeNi@NC.

The anchoring effect of g-C_3N_4 [21], which can successfully prevent metal agglomeration at high temperatures, increase the reactive sites, and improve the catalytic activity, is responsible for the uniform distribution of the numerous spherical nanoparticles with a diameter of about 20 nm that are present on the folded nanosheets (Figure 2b). From the high-resolution TEM (HR-TEM, Figure 2c), lattice stripes in the (111) face of the FeNi alloy can be observed with a face spacing of 0.20 nm, and the region with a lattice spacing of 0.32 nm is associated with the (002) face of graphitic carbon, indicating that the nanoparticles are encapsulated by a carbon layer, and this shell–core structure of the graphitic carbon encapsulated NiFe alloy can effectively prevent the internal alloy from external harsh alkaline environment from corrosion, thus improving the stability of the electrocatalyst, while it effectively facilitates the electron transport [22,23]. The nanosheets, which have superior electron transfer capabilities during electrochemical processes compared to other carbon carriers like one-dimensional carbon fibers, have more channels and a larger specific surface area, which can speed up electron/reactant transport in various directions and expose abundant active sites, favoring catalytic activity [24].

X-ray diffraction (XRD) was used to examine the catalyst's binding mode. The physical phase of this catalyst is the FeNi alloy phase (JPCDS No. 47-1417), as shown in Figure 3a. The diffraction peaks appearing at 2θ = 43.49°, 50.67°, and 74.54° point to the (111), (200), and (220) crystal planes of the FeNi alloy structure, further proving the FeNi alloy's synthesis as shown in Figure 2.

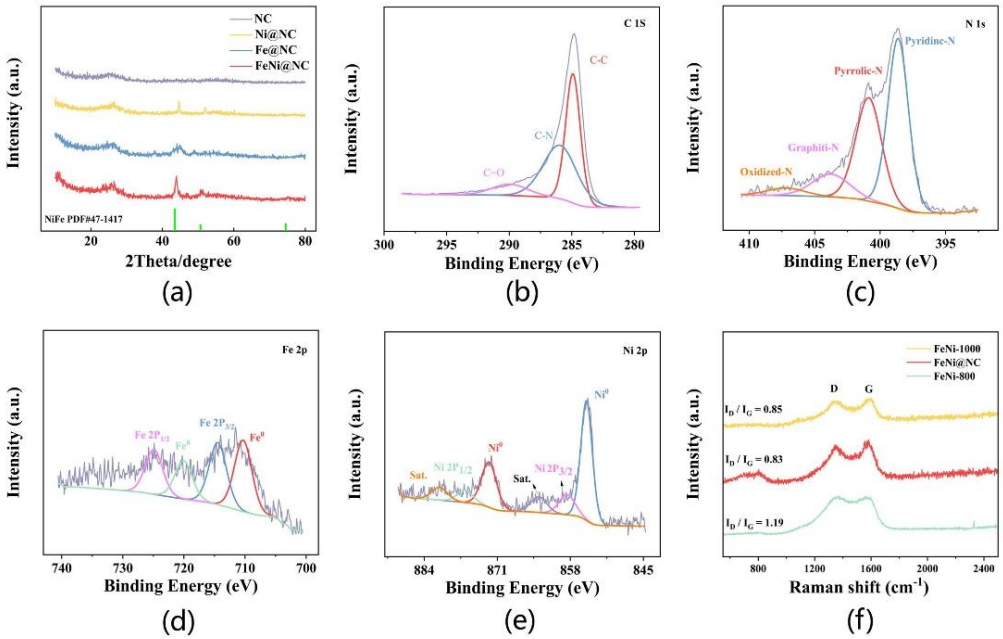

Figure 3. (**a**) XRD patterns of FeNi@NC, high-resolution XPS spectra of (**b**) C 1s, (**c**) N 1s, (**d**) Fe 2p, (**e**) Ni 2p for FeNi@NC. (**f**) Raman spectra of FeNi@NC.

X-ray photoelectron spectroscopy (XPS) was used to examine the surface makeup and chemical phases of the FeNi@NC catalyst. The obtained spectra showed that C (80.81 at%), N (10.29 at%), O (7.08 at%), Fe (0.96 at%), and Ni (0.86 at%) were present. Three different types of bonds were visible in the C 1s XPS spectra (Figure 3b): C-C (284.8 eV), C-N (285.6 eV), and C-O (289.8 eV) [4,23]. The high-resolution N1s XPS peaks for pyridine, pyrrole, and graphitic nitrogen appear in Figure 3c with energies of 398.4, 400.8, and 403.7 eV, respectively. While the N atoms in the graphitic nitrogen are doped within the graphitic carbon plane, it is thought that the pyridine nitrogen, which is present at the edge of the graphitic carbon, functions as an active site for the oxygen reduction reaction (ORR) [25]. The high-resolution XPS Fe 2p and Ni 2p peaks, as shown in Figure 3d,e, revealed the chemical phases of Fe^0 (710.3 eV and 720.0 eV) and Ni^0 (855.0 and 872.5 eV), further verifying the existence of the NiFe alloy [26,27]. Notably, Fe and Ni atoms' ionic states show that Fe-N_x (714.4 and 724.9 eV) and Ni-N_x (858.5 and 876.8 eV) species have formed [27].

The degree of graphitization and the material's ordered/disordered structure can be determined using Raman spectroscopy [28]. A common indication of the level of graphitization in sp2 carbon materials is the intensity ratio of the D (1334 cm^{-1}) to G (1594 cm^{-1}) band (I_D/I_G). As shown in Figure 3f, the ratio of I_D/I_G for FeNi@NC (0.83) is between that of FeNi-800 (1.19) and that of FeNi-1000 (0.85), indicating that FeNi@NC has an intermediate degree of graphitization with some disorder phase, providing necessary defects for catalytic sites [29].

N_2 adsorption–desorption isotherms were used to assess the porosity of the FeNi@NC material. A example Type IV isotherm with a particular surface area of 386.73 m^2g^{-1} was created using the BET approach, as shown in Figure S1. The high gas flow created by the breakdown of g-C_3N_4 during pyrolysis is what causes the huge specific surface area and micropores/mesopores [30,31]. This characteristic enhances the electrocatalytic activity by allowing the catalyst to expose several active sites and exploit the pore structure to transport O_2 and electrolytes to the active sites [32,33].

3.2. Electrocatalytic Activities of FeNi@NC Catalysts for ORR

LSV polarisation curves were performed under standard conditions utilizing an oxygen-saturated 0.1 M KOH electrolyte, a rotating disc electrode (RDE) at 1600 rpm, and a scan rate of 5 mV s^{-1} to assess the electrocatalytic efficacy of FeNi@NC for ORR. LSV tests were also carried out for NC, Ni@NC, Fe@NC, and Pt/C catalysts under the identical conditions to give a parallel comparison. FeNi@NC catalysts were discovered to have an acquired half-wave potential ($E_{1/2}$) of 0.845 V, which is comparable to commercial Pt/C catalysts ($E_{1/2}$ = 0.83 V). Moreover, it is also higher than that of NC ($E_{1/2}$ = 0.77 V) and Ni@NC ($E_{1/2}$ = 0.78 V). Obviously, FeNi@NC electrocatalyst possessed the highest ORR activity. This activity is ascribed to a synergistic interaction between a FeNi alloy and N-doped carbon, which significantly boosts catalytic activity. Additionally, the FeNi@NC final diffusion current density was 6.42 mA cm^{-2} (Figure 4a), demonstrating higher electrocatalytic activity. Due to a lack of Fe and Ni synergy, Ni@NC catalysts only show modest increases in activity [34,35]. At lower potentials, a catalyst with a smaller Tafel slope will be able to achieve a faster charge transfer across the catalytic interface [36], FeNi@NC was also shown to have a smaller Tafel slope (80 mV dec^{-1}) than Pt/C (89 mV dec^{-1}) (Figure 4b). By examining LSV curves produced at various RDE rotation speeds (400–1600 rpm), the kinetics and routes of FeNi@NC in the ORR process were evaluated. The findings demonstrated that the FeNi@NC catalyst's ORR process was kinetically controlled, with the limiting diffusion current density increasing as electrode rotation speed increased (Figure 4c), as a result of the O_2 diffusion distance becoming shorter at faster speeds [37,38]. It was determined that the electron transfer number(n) is a crucial indicator of the catalyst's ORR activity. Using the K-L equation, it has been calculated that the electron transfer number(n) of FeNi@NC was close to 4.0 (Figure 4d), suggesting a four-electron reaction pathway for ORR [39,40].

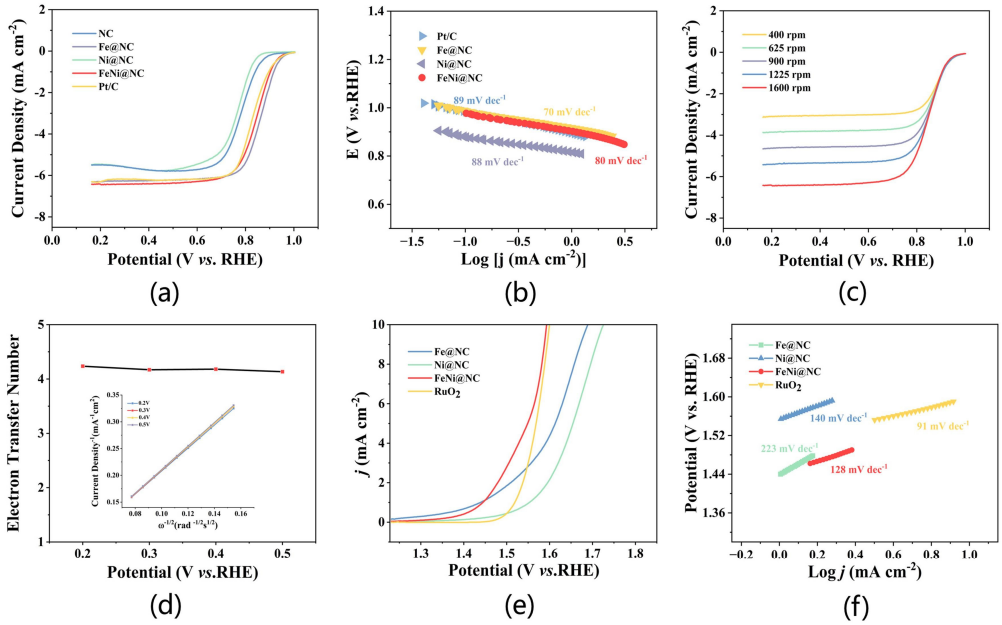

Figure 4. Electrocatalytic ORR performance in 0.1 M KOH. (**a**) ORR LSV curves of NC, Fe@NC, Ni@NC, FeNi@NCand Pt/C in the O_2-saturated 0.1 M KOH electrolyte at 1600 rpm and (**b**) corresponding Tafel plots. (**c**) LSV curves of FeNi@NC at different rotating rates. (**d**) Electron transfer number and the inset shows the K-L plots at different potentials (0.2–0.5 V). (**e**) OER LSV curves and (**f**) Tafel plots of Fe@NC, Ni@NC, FeNi@NC, and RuO_2 in O_2-saturated 1 M KOH.

3.3. OER Performance on FeNi@NC Catalyst

FeNi@NC's OER catalytic activity was thoroughly evaluated. FeNi@NC's OER catalytic activity was carefully evaluated. The overpotential of the FeNi@NC catalyst is shown in Figure 4e at a current density of 10 mA cm^{-2} (360 mV vs. RHE), much lower than that of Ni@NC (490 mV vs. RHE) and Fe@NC (460 mV vs. RHE), and comparable to the noble metal, RuO_2 (370 mV vs. RHE), demonstrating the superior catalytic performance of bimetallic catalysts. This is explained by the creation of Fe–Ni atomic bonds, which cause the charge on Fe and Ni atoms to be redistributed, boosting electrical conductivity and enhancing adsorption strength [41]. As the N-C species alone exhibit low OER activity, FeNi@NC's high OER electrocatalytic activity may also be a result of the contribution of FeNi alloy nanoparticles and the synergistic effect of Fe-N_x/Ni-N_x sites [42,43]. The Tafel slope analysis shown in Figure 4f suggests that the kinetic performance of FeNi@NC is close to that of the noble metal RuO_2 and comparable to Ni@NC and Fe@NC [44–47].

The findings of this work show that when compared to Ni@NC and Fe@NC, FeNi@NC demonstrates superior bifunctional catalytic activity. Table S1 shows this is comparable to other bifunctional ORR/OER catalysts. This activity is ascribed to a synergistic interaction between a FeNi alloy and N-doped carbon, which significantly boosts catalytic activity. Additionally, the distinctive, slightly curled, and mutually supported nanosheet structure of FeNi@NC produces a sizable specific surface area, exposing a greater quantity of active sites and greatly facilitating mass/charge transfer at the interface.

3.4. Application of FeNi@NC in RZABs

The potential use of the synthesized FeNi@NC bifunctional electrocatalyst on ZABs was further assessed due to its excellent catalytic activity. As shown in Figure 5a, RZABs were first put together. These RZABs included polished Zn sheets acting as negative electrodes, air acting as positive electrode, and septa. The electrolytes were 6.0 M KOH and 0.2 M $Zn(CH_3COO)_2$ solutions. $Zn(CH_3COO)_2$ was added to enable the negative electrode's reversible response during repeated charging. The charge/discharge polarization curves of the FeNi@NC-supported cell are shown in Figure 5b, compared to that of a reference

catalyst containing Pt/C + RuO_2 (1.22 V at 50 mA cm^{-2}). The former displayed a reduced charge/discharge voltage gap (1.04 V at 50 mA cm^{-2}), demonstrating the constructed cells' superior charge/discharge capacity. In comparison to Pt/C + RuO_2, the RZABs display much greater open circuit voltage (Voc) and maximum power density. In particular, the maximum power density of FeNi@NC-based RZABs is 116 mW cm^{-2} (Figure 5c), which is higher than the maximum power density of Pt/C + RuO_2 (63 mW cm^{-2}). This is because the Voc of FeNi@NC-based RZABs is 1.45 V, which is higher than the Voc of Pt/C + RuO_2 (1.41 V).

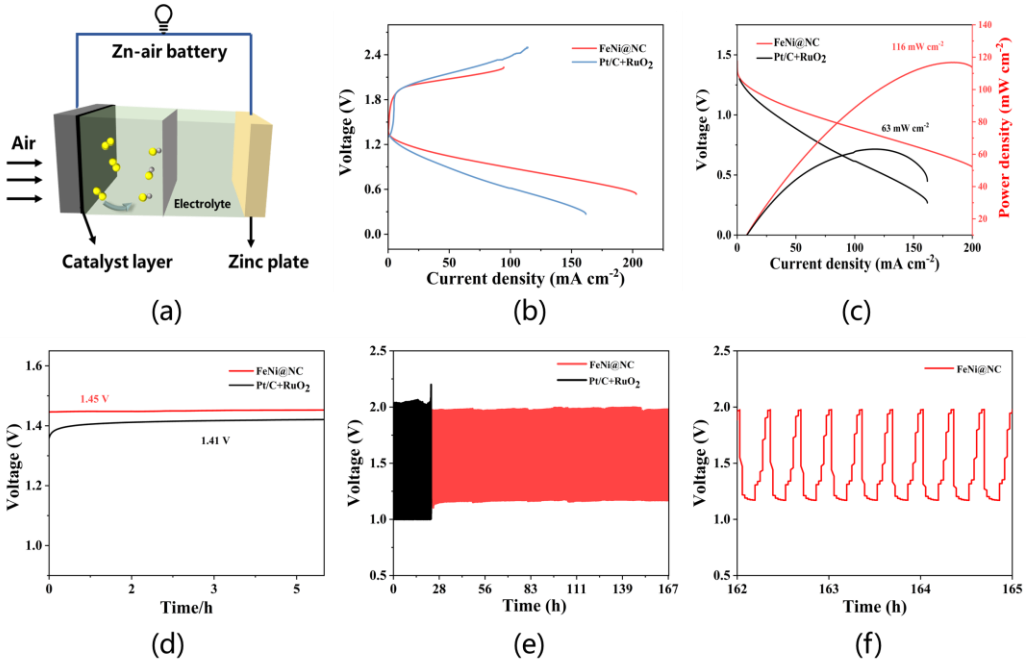

Figure 5. (**a**) Structure of assembled Zn–air batteries. (**b**) Discharge and charge polarization curves. (**c**) Polarization curves and power density curves. (**d**) Open circuit voltage curve. (**e**) Charge and discharge voltage cycling curves at a current density of 10 mA cm^{-2}. (**f**) Enlarged cycle voltage profiles of ZABs with the FeNi@NC cathode.

The data from this evaluation of the RZABs ' charge/discharge performance and cycle stability utilizing the discharging–charging curves is shown in Figure 5e. The FeNi@NC-based RZABs clearly outperform Pt/C + RuO_2-based cells, which showed a noticeable decline in energy conversion efficiency after only 25 h of charge and discharge, as shown by the constant voltage plateau and high energy conversion efficiency after 167 h of charge and discharge at a current density of 10 mA cm^{-2}. Precious metals may tarnish and disappear as a result of charging and discharging [48]. Due to the graphene shell's capacity to effectively stop the alloy from corroding in alkaline circumstances, FeNi@NC has high cycling stability [49]. FeNi@NC-based RZABs have both excellent cycling stability and high maximum power density, which is better than most FeNi-containing RZABs (as shown in Table 1).

Table 1. Comparison of the catalytic characters of the built Zn–air battery with other previous non-noble, metal-based counterparts.

Catalysts	Mass Loading (mg cm^{-2})	Open Circuit Potential (V)	Power Density (mW cm^{-2})	Durability (h)	References
FeNi@NC	1.0	1.45	116	30 min/cycle for 232 cycles; 116 h	This work
FeNi-NC	/	/	80.8	23 h	[50]
Fe-enriched-$FeNi_3$/NC	1.0	1.43	89	10 min/cycle for 100 cycles; 16.7 h	[51]
FeNi/NC	1.0	/	80.5	/	[52]

Table 1. *Cont.*

Catalysts	Mass Loading (mg cm^{-2})	Open Circuit Potential (V)	Power Density (mW cm^{-2})	Durability (h)	References
NiCoFe@N-CNFs	1.0	1.32	147	20 min/cycle for 120 cycles; 40 h	[53]
$Fe_{0.5}Ni_{0.5}$@N-GR	2.0	1.482	85	20 min/cycle for 120 cycles; 40 h	[54]
NiFe/N-CNT	1.5	1.48	300.7	300 cycles; 100 h	[55]
FeNi-N/C-1000	4.0	1.445	102	95 h	[56]
FeNi@N-CNT/NCSs	1.0	1.49	103	2 h/cycle for 30 cycles; 60 h	[57]
NiFe/NCNF/CC	/	/	140.1	700 cycles	[58]
NiFe@NCNT	/	1.48	360.1	5 min/cycle for 2400 cycles; 200 h	[59]
1.5FeNi@NCNT	/	1.44	114	100 cycles	[60]

4. Conclusions

In summary, we created a straightforward, synthetic procedure to create FeNi@NC as a bifunctional catalyst for RZABs. The optimized FeNi@NC has shown an $E_{1/2}$ of 0.845 V and an overpotential of 360 mV at 10 mA cm^{-2}. With a high open circuit voltage of 1.45 V and a power density of 116 mW cm^{-2}, FeNi@NC stands out for the outstanding performance in RZABs. With FeNi nanoalloys serving as the primary catalytic active center, the nitrogen-doped carbon carrier interacts with the FeNi nanoalloys and further enhance the catalytic activity. This research can serve as a useful guide for the development of low-cost, highly effective, and stable bifunctional catalysts.

Supplementary Materials: The following supporting information can be downloaded at: https://www.mdpi.com/article/10.3390/inorganics11070300/s1, Figure S1: N_2 sorption isotherms of FeNi@NC, Table S1: Comparison of the ORR/OER catalytic data of the FeNi@NC with other Previously published FeNi-based catalysts. References [61,62] are cited in the supplementary materials.

Author Contributions: Conceptualization, methodology, writing—original draft preparation, L.D.; data curation, Z.R.; resources, X.C.; project administration, writing—review and editing, D.Z.; methodology, S.X. All authors have read and agreed to the published version of the manuscript.

Funding: This research was funded by National Natural Science Foundation of China grant number [No. 21978193].

Data Availability Statement: Data available on request due to restrictions e.g. privacy. The data presented in this study are available on request from the corresponding author.

Conflicts of Interest: The authors declare no conflict of interest.

References

1. Chen, H.; Liang, X.; Liu, Y.; Ai, X.; Asefa, T.; Zou, X. Active Site Engineering in Porous Electrocatalysts. *Adv. Mater.* **2020**, *32*, e2002435. [CrossRef]
2. Sun, Y.; Zhang, X.; Luo, M.; Chen, X.; Wang, L.; Li, Y.; Li, M.; Qin, Y.; Li, C.; Xu, N.; et al. Ultrathin PtPd-Based Nanorings with Abundant Step Atoms Enhance Oxygen Catalysis. *Adv. Mater.* **2018**, *30*, e1802136. [CrossRef] [PubMed]
3. Kuo, D.Y.; Kawasaki, J.K.; Nelson, J.N.; Kloppenburg, J.; Hautier, G.; Shen, K.M.; Schlom, D.G.; Suntivich, J. Influence of Surface Adsorption on the Oxygen Evolution Reaction on IrO(2)(110). *J. Am. Chem. Soc.* **2017**, *139*, 3473–3479. [CrossRef] [PubMed]
4. Zhang, H.; Zhao, M.; Liu, H.; Shi, S.; Wang, Z.; Zhang, B.; Song, L.; Shang, J.; Yang, Y.; Ma, C.; et al. Ultrastable FeCo Bifunctional Electrocatalyst on Se-Doped CNTs for Liquid and Flexible All-Solid-State Rechargeable Zn-Air Batteries. *Nano Lett.* **2021**, *21*, 2255–2264. [CrossRef]
5. Xu, X.; Xie, J.; Liu, B.; Wang, R.; Liu, M.; Zhang, J.; Liu, J.; Cai, Z.; Zou, J. PBA-derived FeCo alloy with core-shell structure embedded in 2D N-doped ultrathin carbon sheets as a bifunctional catalyst for rechargeable Zn-air batteries. *Appl. Catal. B Environ.* **2022**, *316*, 121687. [CrossRef]
6. Niu, W.; Pakhira, S.; Marcus, K.; Li, Z.; Mendoza-Cortes, J.L.; Yang, Y. Apically Dominant Mechanism for Improving Catalytic Activities of N-Doped Carbon Nanotube Arrays in Rechargeable Zinc-Air Battery. *Adv. Energy Mater.* **2018**, *8*, 1800480. [CrossRef]
7. Wu, M.; Zhang, G.; Hu, Y.; Wang, J.; Sun, T.; Regier, T.; Qiao, J.; Sun, S. Graphitic-shell encapsulated FeNi alloy/nitride nanocrystals on biomass-derived N-doped carbon as an efficient electrocatalyst for rechargeable Zn-air battery. *Carbon. Energy* **2020**, *3*, 176–187. [CrossRef]

8. Yin, J.; Jin, J.; Liu, H.; Huang, B.; Lu, M.; Li, J.; Liu, H.; Zhang, H.; Peng, Y.; Xi, P.; et al. NiCo(2) O(4)-Based Nanosheets with Uniform 4 nm Mesopores for Excellent Zn-Air Battery Performance. *Adv. Mater.* **2020**, *32*, e2001651. [CrossRef]
9. An, L.; Huang, B.; Zhang, Y.; Wang, R.; Zhang, N.; Dai, T.; Xi, P.; Yan, C.H. Interfacial Defect Engineering for Improved Portable Zinc–Air Batteries with a Broad Working Temperature. *Angew. Chem. Int. Ed.* **2019**, *58*, 9459–9463. [CrossRef]
10. Zhu, C.; Shi, Q.; Xu, B.Z.; Fu, S.; Wan, G.; Yang, C.; Yao, S.; Song, J.; Zhou, H.; Du, D.; et al. Hierarchically Porous M–N–C (M = Co and Fe) Single-Atom Electrocatalysts with Robust MNx Active Moieties Enable Enhanced ORR Performance. *Adv. Energy Mater.* **2018**, *8*, 1801956. [CrossRef]
11. Wan, W.; Zhao, Y.; Wei, S.; Triana, C.A.; Li, J.; Arcifa, A.; Allen, C.S.; Cao, R.; Patzke, G.R. Mechanistic insight into the active centers of single/dual-atom Ni/Fe-based oxygen electrocatalysts. *Nat. Commun.* **2021**, *12*, 5589. [CrossRef] [PubMed]
12. Gao, M.; Sheng, W.; Zhuang, Z.; Fang, Q.; Gu, S.; Jiang, J.; Yan, Y. Efficient water oxidation using nanostructured alpha-nickel-hydroxide as an electrocatalyst. *J. Am. Chem. Soc.* **2014**, *136*, 7077–7084. [CrossRef] [PubMed]
13. Li, Y.-y.; Zou, Q.; Li, Z.; Xie, D.; Niu, Y.; Zou, J.; Zeng, X.; Huang, J. MOF derived Ni-Fe based alloy carbon materials for efficient bifunctional electrocatalysts applied in Zn-air battery. *Appl. Surf. Sci.* **2022**, *572*, 151286. [CrossRef]
14. Hu, H.; Meng, Y.; Mei, Y.; Hou, P.X.; Liu, C.; Cheng, H.M.; Shao, M.; Li, J.C. Bifunctional oxygen electrocatalysts enriched with single Fe atoms and NiFe2O4 nanoparticles for rechargeable zinc–air batteries. *Energy Storage Mater.* **2023**, *54*, 517–523. [CrossRef]
15. Lin, S.Y.; Zhang, X.; Sang, S.Y.; Zhang, L.; Feng, J.J.; Wang, A.J. Bio-derived FeNi alloy confined in N-doped carbon nanosheets as efficient air electrodes for Zn-air battery. *J. Colloid. Interface Sci.* **2022**, *628*, 499–507. [CrossRef]
16. Ren, J.-T.; Wang, Y.-S.; Chen, L.; Gao, L.-J.; Tian, W.-W.; Yuan, Z.-Y. Binary FeNi phosphides dispersed on N,P-doped carbon nanosheets for highly efficient overall water splitting and rechargeable Zn-air batteries. *Chem. Eng. J.* **2020**, *389*, 124408. [CrossRef]
17. Zhang, H.; Lv, R. Defect engineering of two-dimensional materials for efficient electrocatalysis. *J. Mater.* **2018**, *4*, 95–107. [CrossRef]
18. Chen, W.; Pei, J.; He, C.T.; Wan, J.; Ren, H.; Wang, Y.; Dong, J.; Wu, K.; Cheong, W.C.; Mao, J.; et al. Single Tungsten Atoms Supported on MOF-Derived N-Doped Carbon for Robust Electrochemical Hydrogen Evolution. *Adv. Mater.* **2018**, *30*, e1800396. [CrossRef]
19. Wang, M.Q.; Ye, C.; Liu, H.; Xu, M.; Bao, S.J. Nanosized Metal Phosphides Embedded in Nitrogen-Doped Porous Carbon Nanofibers for Enhanced Hydrogen Evolution at All pH Values. *Angew. Chem. Int. Ed. Engl.* **2018**, *57*, 1963–1967. [CrossRef]
20. Fu, Y.; Yu, H.-Y.; Jiang, C.; Zhang, T.-H.; Zhan, R.; Li, X.; Li, J.-F.; Tian, J.-H.; Yang, R. NiCo Alloy Nanoparticles Decorated on N-Doped Carbon Nanofibers as Highly Active and Durable Oxygen Electrocatalyst. *Adv. Funct. Mater.* **2018**, *28*, 1705094. [CrossRef]
21. Zhao, L.; Zhang, Y.; Huang, L.B.; Liu, X.Z.; Zhang, Q.H.; He, C.; Wu, Z.Y.; Zhang, L.J.; Wu, J.; Yang, W.; et al. Cascade anchoring strategy for general mass production of high-loading single-atomic metal-nitrogen catalysts. *Nat. Commun.* **2019**, *10*, 1278. [CrossRef]
22. Deng, J.; Ren, P.; Deng, D.; Bao, X. Enhanced electron penetration through an ultrathin graphene layer for highly efficient catalysis of the hydrogen evolution reaction. *Angew. Chem. Int. Ed. Engl.* **2015**, *54*, 2100–2104. [CrossRef]
23. Zou, L.; Hou, C.C.; Wang, Q.; Wei, Y.S.; Liu, Z.; Qin, J.S.; Pang, H.; Xu, Q. A Honeycomb-Like Bulk Superstructure of Carbon Nanosheets for Electrocatalysis and Energy Storage. *Angew. Chem. Int. Ed. Engl.* **2020**, *59*, 19627–19632. [CrossRef]
24. Liu, S.J.; Amiinu, I.S.; Liu, X.B.; Zhang, J.; Bao, M.J.; Meng, T.; Mu, S.C. Carbon nanotubes intercalated Co/N-doped porous carbon nanosheets as efficient electrocatalyst for oxygen reduction reaction and zinc-air batteries. *Chem. Eng. J.* **2018**, *342*, 163–170. [CrossRef]
25. Han, S.; Hu, X.; Wang, J.; Fang, X.; Zhu, Y. Novel Route to Fe-Based Cathode as an Efficient Bifunctional Catalysts for Rechargeable Zn-Air Battery. *Adv. Energy Mater.* **2018**, *8*, 1800955. [CrossRef]
26. Li, T.; Luo, G.; Liu, K.; Li, X.; Sun, D.; Xu, L.; Li, Y.; Tang, Y. Encapsulation of Ni_3Fe Nanoparticles in N-Doped Carbon Nanotube-Grafted Carbon Nanofibers as High-Efficiency Hydrogen Evolution Electrocatalysts. *Adv. Funct. Mater.* **2018**, *28*, 1805828. [CrossRef]
27. Tong, M.; Wang, L.; Fu, H. Designed Synthesis and Catalytic Mechanisms of Non-Precious Metal Single-Atom Catalysts for Oxygen Reduction Reaction. *Small Methods* **2021**, *5*, e2100865. [CrossRef]
28. Liu, J.; Xie, J.; Wang, R.; Liu, B.; Meng, X.; Xu, X.; Tang, B.; Cai, Z.; Zou, J. Interfacial electron modulation of Cu_2O by Co_3O_4 embedded in hollow carbon cube skeleton for boosting oxygen reduction/revolution reactions. *Chem. Eng. J.* **2022**, *450*, 137961. [CrossRef]
29. Li, Y.; Liu, Q.; Zhang, S.; Li, G. The Vital Balance of Graphitization and Defect Engineering for Efficient Bifunctional Oxygen Electrocatalyst Based on N-doping Carbon/CNT Frameworks. *Chemcatchem* **2019**, *11*, 861–867. [CrossRef]
30. Ong, W.J.; Tan, L.L.; Ng, Y.H.; Yong, S.T.; Chai, S.P. Graphitic Carbon Nitride (g-C3N4)-Based Photocatalysts for Artificial Photosynthesis and Environmental Remediation: Are We a Step Closer To Achieving Sustainability? *Chem. Rev.* **2016**, *116*, 7159–7329. [CrossRef]
31. Tian, B.; Ho, D.; Qin, J.; Hu, J.; Chen, Z.; Voiry, D.; Wang, Q.; Zeng, Z. Framework structure engineering of polymeric carbon nitrides and its recent applications. *Prog. Mater. Sci.* **2023**, *133*, 101056. [CrossRef]
32. Lee, S.H.; Kim, J.; Chung, D.Y.; Yoo, J.M.; Lee, H.S.; Kim, M.J.; Mun, B.S.; Kwon, S.G.; Sung, Y.E.; Hyeon, T. Design Principle of Fe-N-C Electrocatalysts: How to Optimize Multimodal Porous Structures? *J. Am. Chem. Soc.* **2019**, *141*, 2035–2045. [CrossRef] [PubMed]

33. Wan, W.; Liu, X.; Li, H.; Peng, X.; Xi, D.; Luo, J. 3D carbon framework-supported CoNi nanoparticles as bifunctional oxygen electrocatalyst for rechargeable Zn-air batteries. *Appl. Catal. B Environ.* **2019**, *240*, 193–200. [CrossRef]
34. Deng, C.; Wu, K.-H.; Scott, J.; Zhu, S.; Amal, R.; Wang, D.-W. Ternary MnO/CoMn alloy@N-doped graphitic composites derived from a bi-metallic pigment as bi-functional electrocatalysts. *J. Mater. Chem. A* **2019**, *7*, 20649–20657. [CrossRef]
35. Gupta, S.; Qiao, L.; Zhao, S.; Xu, H.; Lin, Y.; Devaguptapu, S.V.; Wang, X.; Swihart, M.T.; Wu, G. Highly Active and Stable Graphene Tubes Decorated with FeCoNi Alloy Nanoparticles via a Template-Free Graphitization for Bifunctional Oxygen Reduction and Evolution. *Adv. Energy Mater.* **2016**, *6*, 1601198. [CrossRef]
36. Niu, W.; Li, L.; Liu, X.; Wang, N.; Liu, J.; Zhou, W.; Tang, Z.; Chen, S. Mesoporous N-doped carbons prepared with thermally removable nanoparticle templates: An efficient electrocatalyst for oxygen reduction reaction. *J. Am. Chem. Soc.* **2015**, *137*, 5555–5562. [CrossRef]
37. Song, J.; Ren, Y.; Li, J.; Huang, X.; Cheng, F.; Tang, Y.; Wang, H. Core-shell Co/CoNx@C nanoparticles enfolded by Co-N doped carbon nanosheets as a highly efficient electrocatalyst for oxygen reduction reaction. *Carbon* **2018**, *138*, 300–308. [CrossRef]
38. Kuang, M.; Wang, Q.; Han, P.; Zheng, G. Cu, Co-Embedded N-Enriched Mesoporous Carbon for Efficient Oxygen Reduction and Hydrogen Evolution Reactions. *Adv. Energy Mater.* **2017**, *7*, 1700193. [CrossRef]
39. Niu, J.; Geng, C.; Liu, X.; O'Mullane, A.P. Transformation of a new polyoxometalate into multi-metal active sites on ZIF-derived carbon nanotubes as bifunctional cathode catalyst and dendrite-free anode coating for Zn-air batteries. *Chem. Eng. J.* **2023**, *468*, 143607. [CrossRef]
40. Weng, P.; Guo, Y.; Wu, K.; Wang, X.; Huang, G.-Q.; Lei, H.; Yuan, Y.; Lu, W.; Li, D. Design of Fe/Ni-doped N/S-rich carbon with advanced bifunctional electrocatalysis for Zn–air batteries. *J. Mater. Chem. A* **2023**, *11*, 12194–12201. [CrossRef]
41. Zhu, X.; Zhang, D.; Chen, C.-J.; Zhang, Q.; Liu, R.-S.; Xia, Z.; Dai, L.; Amal, R.; Lu, X. Harnessing the interplay of Fe–Ni atom pairs embedded in nitrogen-doped carbon for bifunctional oxygen electrocatalysis. *Nano Energy* **2020**, *71*, 104597. [CrossRef]
42. Lai, C.; Wang, J.; Lei, W.; Xuan, C.; Xiao, W.; Zhao, T.; Huang, T.; Chen, L.; Zhu, Y.; Wang, D. Restricting Growth of Ni_3Fe Nanoparticles on Heteroatom-Doped Carbon Nanotube/Graphene Nanosheets as Air-Electrode Electrocatalyst for Zn-Air Battery. *ACS Appl. Mater. Interfaces* **2018**, *10*, 38093–38100. [CrossRef] [PubMed]
43. Zheng, J.; Kang, T.; Liu, B.; Wang, P.; Li, H.; Yang, M. N-doped carbon nanotubes encapsulated with FeNi nanoparticles derived from defect-rich, molecule-doped 3D g-C3N4 as an efficient bifunctional electrocatalyst for rechargeable zinc–air batteries. *J. Mater. Chem. A* **2022**, *10*, 9911–9921. [CrossRef]
44. Yu, Y.; You, S.; Du, J.; Xing, Z.; Dai, Y.; Chen, H.; Cai, Z.; Ren, N.; Zou, J. ZIF-67-derived CoO (tetrahedral Co^{2+})@nitrogen-doped porous carbon protected by oxygen vacancies-enriched SnO_2 as highly active catalyst for oxygen reduction and Pt co-catalyst for methanol oxidation. *Appl. Catal. B Environ.* **2019**, *259*, 118043. [CrossRef]
45. Li, W.; Chen, Y.; Yu, B.; Hu, Y.; Wang, X.; Yang, D. 3D hollow Co-Fe-P nanoframes immobilized on N,P-doped CNT as an efficient electrocatalyst for overall water splitting. *Nanoscale* **2019**, *11*, 17031–17040. [CrossRef] [PubMed]
46. Liu, L.; Yan, F.; Li, K.; Zhu, C.; Xie, Y.; Zhang, X.; Chen, Y. Ultrasmall FeNi3N particles with an exposed active (110) surface anchored on nitrogen-doped graphene for multifunctional electrocatalysts. *J. Mater. Chem. A* **2019**, *7*, 1083–1091. [CrossRef]
47. Wang, J.; Ciucci, F. Boosting Bifunctional Oxygen Electrolysis for N-Doped Carbon via Bimetal Addition. *Small* **2017**, *13*, 1604103. [CrossRef]
48. Tang, C.; Wang, B.; Wang, H.F.; Zhang, Q. Defect Engineering toward Atomic Co-Nx -C in Hierarchical Graphene for Rechargeable Flexible Solid Zn-Air Batteries. *Adv. Mater.* **2017**, *29*, 1703185. [CrossRef]
49. Wang, R.; Liu, B.; You, S.; Li, Y.; Zhang, Y.; Wang, D.; Tang, B.; Sun, Y.; Zou, J. Three-dimensional Ni3Se4 flowers integrated with ultrathin carbon layer with strong electronic interactions for boosting oxygen reduction/evolution reactions. *Chem. Eng. J.* **2022**, *430*, 132720. [CrossRef]
50. Yang, L.; Zeng, X.F.; Wang, D.; Cao, D.P. Biomass-derived FeNi alloy and nitrogen-codoped porous carbons as highly efficient oxygen reduction and evolution bifunctional electrocatalysts for rechargeable Zn-air battery. *Energy Storage Mater.* **2018**, *12*, 277–283. [CrossRef]
51. Chen, K.; Kim, S.; Rajendiran, R.; Prabakar, K.; Li, G.Z.; Shi, Z.C.; Jeong, C.; Kang, J.; Li, O.L. Enhancing ORR/OER active sites through lattice distortion of Fe-enriched $FeNi_3$ intermetallic nanoparticles doped N-doped carbon for high-performance rechargeable Zn-air battery. *J. Colloid. Interface Sci.* **2021**, *582*, 977–990. [CrossRef] [PubMed]
52. Li, G.L.; Xu, X.C.; Yang, B.B.; Cao, S.; Wang, X.Y.; Fu, X.D.; Shi, Y.T.; Yan, Y.; Song, X.D.; Hao, C. Micelle-template synthesis of a 3D porous FeNi alloy and nitrogen-codoped carbon material as a bifunctional oxygen electrocatalyst. *Electrochim. Acta* **2020**, *331*, 135375. [CrossRef]
53. Cao, F.; Yang, X.; Shen, C.; Li, X.; Wang, J.M.; Qin, G.W.; Li, S.; Pang, X.Y.; Li, G.Q. Electrospinning synthesis of transition metal alloy nanoparticles encapsulated in nitrogen-doped carbon layers as an advanced bifunctional oxygen electrode. *J. Mater. Chem. A* **2020**, *8*, 7245–7252. [CrossRef]
54. Liu, P.T.; Gao, D.Q.; Xiao, W.; Ma, L.; Sun, K.; Xi, P.X.; Xue, D.S.; Wang, J. Self-powered water-splitting devices by core–shell NiFe@N-graphite-based Zn–air batteries. *Adv. Funct. Mater.* **2018**, *28*, 1706928. [CrossRef]
55. Lei, H.; Wang, Z.L.; Yang, F.; Huang, X.Q.; Liu, J.H.; Liang, Y.Y.; Xie, J.P.; Javed, M.S.; Lu, X.H.; Tan, S.Z.; et al. NiFe nanoparticles embedded N-doped carbon nanotubes as high-efficient electrocatalysts for wearable solid-state Zn-air batteries. *Nano Energy* **2020**, *68*, 104293. [CrossRef]

56. Cui, J.; Leng, Y.M.; Xiang, Z.H. FeNi co-doped electrocatalyst synthesized via binary ligand strategy as a bifunctional catalyst for Zn-air flow battery. *Chem. Eng. Sci.* **2022**, *247*, 117038. [CrossRef]
57. Ren, J.T.; Chen, L.; Wang, Y.S.; Tian, W.W.; Gao, L.J.; Yuan, Z.Y. FeNi nanoalloys encapsulated in N-doped cnts tangled with n-doped carbon nanosheets as efficient multifunctional catalysts for overall water splitting and rechargeable Zn–air batteries. *ACS Sustain. Chem. Eng.* **2020**, *8*, 223–237. [CrossRef]
58. Lai, C.L.; Fang, J.Y.; Liu, X.P.; Gong, M.X.; Zhao, T.H.; Shen, T.; Wang, K.L.; Jiang, K.; Wang, D.L. In situ coupling of NiFe nanoparticles with N-doped carbon nanofibers for Zn-air batteries driven water splitting. *Appl. Catal. B Environ.* **2021**, *285*, 119856. [CrossRef]
59. Jiang, M.X.; Tan, Z.; Cao, M.H. A robust bifunctional electrocatalyst for rechargeable zinc-air batteries: NiFe nanoparticles encapsulated in nitrogen-doped carbon nanotubes. *Int. J. Hydrogen Energ.* **2021**, *46*, 15507–15516. [CrossRef]
60. Wu, M.C.; Guo, B.K.; Nie, A.M.; Liu, R. Tailored architectures of FeNi alloy embedded in N-doped carbon as bifunctional oxygen electrocatalyst for rechargeable zinc-air battery. *J. Colloid. Interface Sci.* **2020**, *561*, 585–592. [CrossRef]
61. Zheng, X.J.; Cao, X.C.; Zeng, K.; Yan, J.; Sun, Z.; Ruemmeli, M.H.; Yang, R. A self-jet vapor-phase growth of 3D FeNi@NCNT clusters as efficient oxygen electrocatalysts for zinc-air batteries. *Small* **2021**, *17*, 2006183. [CrossRef] [PubMed]
62. Chen, D.; Li, G.F.; Chen, X.; Zhang, Q.; Sui, J.; Li, C.; Zhang, Y.; Hu, J.; Yu, J.; Yu, L.; et al. Developing nitrogen and Co/Fe/Ni multi-doped carbon nano-tubes as high-performance bifunctional catalyst for rechargeable zinc-air battery. *J. Colloid. Interface Sci.* **2021**, *593*, 204–213. [CrossRef] [PubMed]